In press On The Astrophysical Journal Letters
Preprint typeset using LaTeX style emulateapj v. 11/10/09

arXiv:1404.2607v1 [astro-ph.CO] 9 Apr 2014

A NEW COSMOLOGICAL DISTANCE MEASURE USING AGN X-RAY VARIABILITY

Fabio La Franca[1,2], Stefano Bianchi[1], Gabriele Ponti[3], Enzo Branchini[1,2,4], and Giorgio Matt[1]

Received 2014 March 18; accepted 2014 April 8

ABSTRACT

We report the discovery of a luminosity distance estimator using Active Galactic Nuclei (AGN). We combine the correlation between the X-ray variability amplitude and the Black Hole (BH) mass with the single epoch spectra BH mass estimates which depend on the AGN luminosity and the line width emitted by the broad line region. We demonstrate that significant correlations do exist which allows one to predict the AGN (optical or X-ray) luminosity as a function of the AGN X-ray variability and either the Hβ or the Paβ line widths. In the best case, when the Paβ is used, the relationship has an intrinsic dispersion of $\sim$0.6 dex. Although intrinsically more disperse than Supernovae Ia, this relation constitutes an alternative distance indicator potentially able to probe, in an independent way, the expansion history of the Universe. With this respect, we show that the new mission concept *Athena* should be able to measure the X-ray variability of hundreds of AGN and then constrain the distance modulus with uncertainties of 0.1 mag up to $z \sim 0.6$. We also discuss how, using a new dedicated wide field X-ray telescope able to measure the variability of thousands of AGNs, our estimator has the prospect to become a cosmological probe even more sensitive than current Supernovae Ia samples.

Subject headings: distance scale — cosmological parameters — cosmology: observations — Galaxies: active — X-rays: general

1. INTRODUCTION

One of the most important results on observational cosmology is the discovery, using type Ia supernovae (SNeIa) as standard candles, of the accelerating expansion of the Universe (Riess et al. 1998; Perlmutter et al. 1999). However, the use of SNeIa is difficult beyond $z \sim 1$ and limited up to $z \sim 2$ (e.g. Rubin et al. 2013). It is therefore of paramount importance to calibrate other independent distance indicators able to measure the Universe expansion. It would be even better if such a method would be able to probe even beyond these redshifts, where the differences among various cosmological models are larger.

Given their high luminosities, since their discovery there have been several studies on the use of Active Galactic Nuclei (AGN) as standard candles or rulers (Baldwin 1977; Rudge & Raine 1999; Collier et al. 1999; Elvis & Karovska 2002). More recently, also thanks to a better understanding of the AGN structure, more promising methods have been presented (see Marziani & Sulentic (2013) and the review therein). For example, many authors (e.g. Watson et al. 2011) use the tight relationship between the luminosity of an AGN and the radius of its Broad Line Region (BLR) established via reverberation mapping to determine the luminosity distances. On the other hand, Wang et al. (2013) suggest that super-Eddington accreting massive BH may reach saturated luminosities, which then provide a new tool for estimating cosmological distances. Besides AGN, gamma ray bursts (GRB) have been used as standard candles, however their low identification rate makes their use difficult (e.g. Schaefer 2007, and references therein).

Here we propose a new method to predict the AGN luminosity based on the combination of the virial relations, which allow to derive the BH mass (M_{BH}) from the AGN luminosity and the width of the lines emitted from the BLR, and the well established anti-correlation between M_{BH} and the X-ray variability amplitude.

2. METHOD

The method which uses single epoch (SE) spectra (in the optical or near infrared bands) to measure M_{BH} (e.g. Wandel et al. 1999; McLure & Jarvis 2002; Vestergaard & Osmer 2009; Landt et al. 2013) is now well established. By combining the velocity, ΔV, of the BLR clouds (assuming Keplerian orbits) along with their distance R it is possible to determine the total mass contained within the BLR (which is dominated by the BH) using

$$M_{BH} = \frac{f \Delta V^2 R}{G}, \quad (1)$$

where G is the gravitational constant, $\Delta V^2 R$ is the virial product and f is a factor which depends on the geometric and kinematic structure of the BLR. These techniques derive M_{BH} using SE spectra to measure ΔV from the Full Width at Half Maximum (FWHM) of some of the BLR lines (typically: H_β or MgII2798Å or CIV1459Å) and R from either the continuum or the line luminosities, L, which have been proved to be proportional to R^2 (see Bentz et al. 2013, and references therein). Therefore, the SE estimates are based on relations of the type

$$\log M_{BH} = \alpha \log L + \beta \log \Delta V + \gamma, \quad (2)$$

where the values of the parameters $\alpha \sim 0.5$, $\beta \sim 2$ and γ depend on the emission line of the BLR used. These relationships have typical uncertainties of $\sim$0.5 dex.

[1] Dipartimento di Matematica e Fisica, Università Roma Tre, via della Vasca Navale 84, I-00146, Roma, Italy; lafranca,bianchi,branchin,matt@fis.uniroma3.it
[2] INAF - Osservatorio Astronomico di Roma, via Frascati 33, I-00040, Monte Porzio Catone (RM), Italy
[3] Max-Planck-Institut für extraterrestrische Physik, Giessenbachstrasse 1, D-85748 Garching bei München, Germany
[4] INFN - Sezione di Roma Tre, via della Vasca Navale 84, I-00146, Roma, Italy

TABLE 1
Calibration Sample

Name	z	$\sigma^2_{\rm rms}$	low-err$_{\sigma^2_{\rm rms}}$	up-err$_{\sigma^2_{\rm rms}}$	logL$_{5100}$ erg s^{-1}	logL$_{\rm x}$ erg s^{-1}	FWHM$_{H\beta}$ km s^{-1}	FWHM$_{Pa\beta}$ km s^{-1}	Ref
(1)	(2)	(3)	(4)	(5)	(6)	(7)	(8)	(9)	(10)
1E0919+515	0.1610	0.078000	0.052439	0.091463	44.29	43.43	1980	...	a
1H0707-495	0.0411	0.219000	0.027439	0.030488	...	42.67	1000	...	b
3C120	0.0330	0.000210	0.000116	0.000183	44.09	44.06	2327	2733	c
3C273	0.1583	0.000027	0.000022	0.000024	46.02	45.80	3500	2916	d
ARK120	0.0323	0.000290	0.000249	0.000427	44.37	43.96	6120	5114	d
ARK564	0.0247	0.044000	0.008537	0.012195	...	43.37	...	1616	
ESO198-G24	0.0455	0.000780	0.000445	0.000671	...	43.70	6400	...	e
HE1029-1401	0.0860	0.001000	0.000610	0.001159	45.27	44.54	7500	...	f
HE1143-1810	0.0330	0.000690	0.000463	0.000671	...	43.85	2400	...	e
IC4329A	0.0161	0.000168	0.000084	0.000137	42.89	43.75	5964	...	c
IRAS13349+2438	0.1076	0.007300	0.002256	0.004268	44.64	43.87	2800	...	g
IRAS17020+4544	0.0610	0.016400	0.004695	0.007317	...	43.71	1040	...	h
IRASF12397+3333	0.0450	0.009500	0.003049	0.004878	43.36	43.38	1640	...	g
MCG-6-30-15	0.0077	0.035200	0.005000	0.004878	42.86	42.75	2020	...	i
MRK110	0.0353	0.000398	0.000269	0.000410	43.63	43.91	2079	1918	d
MRK1502	0.0611	0.021300	0.005732	0.012195	44.79	43.65	1171	...	d
MRK279	0.0305	0.000275	0.000173	0.000238	43.82	43.78	5411	3568	d
MRK335	0.0258	0.015160	0.002382	0.002382	43.71	43.44	1841	1858	d
MRK509	0.0344	0.000296	0.000093	0.000091	43.91	44.02	3424	3077	l
MRK590	0.0264	0.002154	0.001468	0.002390	44.01	43.04	2627	3964	d
MRK766	0.0129	0.027787	0.003285	0.003285	43.31	42.94	1100	...	g
MRK841	0.0364	0.001700	0.001037	0.001829	43.64	43.49	6000	...	g
NGC3227	0.0039	0.008757	0.001976	0.004366	42.86	41.57	4445	2955	g
NGC3516	0.0088	0.003594	0.001015	0.001015	43.17	42.46	5236	4469	g
NGC3783	0.0097	0.005052	0.001217	0.001217	43.20	43.08	3555	...	d
NGC4051	0.0023	0.113421	0.012172	0.012172	41.47	41.44	1170	1681	l
NGC4151	0.0033	0.000890	0.000427	0.000915	42.58	42.53	6421	4667	d
NGC4395	0.0011	0.144050	0.031327	0.065367	...	40.21	1500	...	m
NGC4593	0.0090	0.009819	0.003163	0.006379	42.85	42.87	5143	3791	c
NGC5548	0.0172	0.000283	0.000173	0.000278	43.21	43.42	6300	6525	l
NGC7469	0.0163	0.002942	0.000641	0.001363	43.74	43.23	2639	1792	d
PDS456	0.1840	0.004800	0.001402	0.001220	...	44.90	3974	2068	n
PG0844+349	0.0640	0.019000	0.010366	0.024390	...	43.70	...	2410	
PG1211+143	0.0809	0.010500	0.002683	0.005488	44.42	43.73	1900	...	g
PG1440+356	0.0791	0.006400	0.002927	0.004878	44.46	43.61	1630	...	g
RE1034+396	0.0421	0.018000	0.006707	0.009756	43.18	42.53	700	...	g
RXJ0057.2-2223	0.0620	0.023000	0.010366	0.018293	44.27	43.65	970	...	g
RXJ0136.9-3510	0.2890	0.064000	0.026220	0.054878	...	44.34	1320	...	o
RXJ0323.2-4931	0.0710	0.009000	0.006707	0.010976	43.58	43.21	1680	...	g
SDSSJ135724.51+652505.9	0.1063	0.073000	0.044512	0.054878	43.14	42.90	737	...	p

Note. — Columns 3, 4 and 5: Excess variance, $\sigma^2_{\rm rms}$, and lower and upper errors at 1σ confidence level from Ponti et al. (2012). Column 6: λL_λ continuum luminosity at 5100Å. Column 7: 2-10 keV intrinsic luminosity. Column 9: from Landt et al. (2008, 2013). Column 10: References for FWHM$_{H\beta}$ and L$_{5100}$: a) Jin et al. (2012), b) Boller et al. (1996), c) Assef et al. (2012), d) Vestergaard & Peterson (2006), e) Winkler (1992), f) McLure & Dunlop (2001), g) Grupe et al. (2004), h) Leighly (1999), i) McHardy et al. (2005), l) Wandel et al. (1999), m) Kraemer et al. (1999), n) Torres et al. (1997), o) Grupe et al. (1999), p) Zhou et al. (2006).

On the other hand, several studies have found a significant anti-correlation between M$_{\rm BH}$ and the X-rays variability (Nandra et al. 1997; Turner et al. 1999; O'Neill et al. 2005; McHardy et al. 2006; Gierliński et al. 2008; Zhou et al. 2010; Ponti et al. 2012; Kelly et al. 2013). Following Ponti et al. (2012) it results

$$\log M_{\rm BH} = -k \cdot \log \sigma^2_{\rm rms} + w, \quad (3)$$

where $k \sim 0.8$ and w are two constants which depend on the time scale and the energy range where the variable flux is measured. σ^2_{rms} is the normalised excess variance variability estimator:

$$\sigma^2_{\rm rms} = \frac{1}{N\mu^2} \Sigma_{i=1}^{N} \left[(X_i - \mu)^2 - \sigma_i^2 \right], \quad (4)$$

where N is the number of time intervals where the fluxes (or the counts) X_i are measured, μ is the mean of the N fluxes X_i and σ_i is the uncertainty on the i-th flux measure. According to X-ray variability studies on samples of AGN whose M$_{\rm BH}$ has been measured with reverberation mapping techniques, these kinds of relationships could have spreads as narrow as 0.2-0.4 dex (Zhou et al. 2010; Ponti et al. 2012; Kelly et al. 2013).

The origin of M$_{\rm BH}$ -$\sigma^2_{\rm rms}$relation (eq. 3) is to be found in the dependence on M$_{\rm BH}$ of the time-scales of what appears to be a universal shape of the AGN variability power spectral density (PSD). Indeed, the AGN X-ray PSDs are generally well modelled by two power laws, P(ν) $\propto 1/\nu^n$, where the PSD slope is $n \sim 1$ down to a break frequency ν_b, that scales primarily with M$_{\rm BH}$, and then steepens to $n \sim 2$ at larger frequencies. However, measuring the shape of the AGN X-ray PSD is very data demanding, requiring high quality data on many different time-scales. Therefore these studies are confined to a relatively small number of sources. On the contrary, the excess variance $\sigma^2_{\rm rms}$ is a robust estimator as it corresponds to the integral of the PSD on the time scales

probed by the data. The scaling of the characteristic frequencies of the PSD with M_{BH} (and the roughly similar PSD normalisation at ν_b) induces a dependence of the excess variance with M_{BH} (if computed at frequencies above ν_b).

The two equations (2 and 3) used to estimate M_{BH} can be combined to derive the intrinsic AGN luminosity as a function of its X-ray variability, σ^2_{rms}, and line width, ΔV:

$$\log L = -\frac{k}{\alpha} \cdot \log\sigma^2 - \frac{\beta}{\alpha}\log\Delta V + \text{const}, \quad (5)$$

which, if we (for the sake of simplicity) assume $\alpha = 0.5$ and $\beta = 2$, becomes

$$\log L = -2k \cdot \log\sigma^2 - 4\log\Delta V + \text{const}. \quad (6)$$

In this work we aim to verify if the above proposed relationship does work and then calibrate it. It should be noted that, in many previous studies, a correlation between the AGN luminosity and X-ray variability has been measured (e.g. Ponti et al. 2012; Shemmer et al. 2014, and references therein). According to the above discussion, we believe that such a correlation is the projection on the L-$\sigma^2_{\rm rms}$ plane of our proposed 3D relationship among L, $\sigma^2_{\rm rms}$ and ΔV (eq. 6). If this is the case, we should measure a more significant and less scattered relation than previously reported using only L and $\sigma^2_{\rm rms}$.

We adopted a flat cosmology with $H_0 = 70$ km s^{-1} Mpc^{-1}, Ω_M=0.30 and Ω_Λ=0.70. Unless otherwise stated, uncertainties are quoted at the 68% (1σ) confidence level.

3. CALIBRATION SAMPLE

We have used the variability measures coming from the XMM-Newton systematic excess variance study of radio quiet, X-ray un-obscured, AGN by Ponti et al. (2012). Light curves have been constructed in the 2-10 keV energy band with t_0=250 s long bins and divided into segments of 20 ks. We selected all those objects whose excess variance, $\sigma^2_{\rm rms}$, was measured with a significance larger than $\sim 1.2\sigma$ and for which the FWHM of the broad component of the Hβ (FWHM$_{\rm H\beta}$) and the λL_λ continuum luminosity at 5100Å, L_{5100}, estimates were available in the literature. For most of the objects, when possible, coeval measures, obtained from the same optical spectra, were used. In addition, we collected the Paβ FWHM measures (FWHM$_{\rm Pa\beta}$) from Landt et al. (2008, 2013), when available. In total the sample contains 40 low redshift AGN (86% with $z < 0.1$), 38 and 18 with Hβ or Paβ line widths measurements available, respectively (in two objects, Ark 564 and PG 0844+349, the Hβ line width and L_{5100} measures are missing, while the Paβ line width is available; see Table 1).

4. THE CALIBRATION FITS

We have performed a linear fit of the relation

$$\log\frac{L}{\text{erg s}^{-1}} + 4\log\frac{\text{FWHM}}{10^3 \text{ km s}^{-1}} = \alpha \cdot \log\sigma^2_{\rm rms} + \beta, \quad (7)$$

(looking for the best fit α and β parameters) using FITEXY (Press et al. 2007) that can incorporate errors on both variables[1]. As a first step we have investigated whether a relationship exists using L_{5100} and FWHM$_{\rm H\beta}$ to build up the virial product. Among the three quantities $\sigma^2_{\rm rms}$, L_{5100} and FWHM$_{\rm H\beta}$, we can ignore the uncertainties on L_{5100} as they are experimentally less than 3%, while the uncertainties on $\sigma^2_{\rm rms}$ are in the range 10-90% (see Table 1 and references therein). As far as the FWHM measures are concerned, and although in some cases the uncertainties are reported in the literature, we have preferred to assume a common uncertainty of 20% following the results of Grupe et al. (2004); Vestergaard & Peterson (2006); Denney et al. (2009); Assef et al. (2012). The data and the results of the fit are shown in Figure 1 and Table 2. The logarithm of the square of the virial product, computed using L_{5100} and FWHM$_{\rm H\beta}$, is strongly correlated with the logarithm of $\sigma^2_{\rm rms}$: the correlation coefficient, r= -0.73, has a probability as low as $\sim 3\times10^{-6}$ that the data are randomly extracted from an uncorrelated parent population. The observed and intrinsic (subtracting in quadrature the data uncertainties) spreads are: 1.12 dex and 1.00 dex, respectively.

A correlation between the AGN luminosity and the X-ray variability (without using the line width of a BLR line as a second parameter) of the type

$$\log\frac{L}{\text{erg s}^{-1}} = \alpha' \cdot \log\sigma^2_{\rm rms} + \beta', \quad (8)$$

was already reported (e.g. Ponti et al. 2012, and references therein). If the same sample is used, the linear correlation between logL_{5100} and log$\sigma^2_{\rm rms}$has a spread of 1.78 dex (instead of 1.12 dex) while the correlation coefficient is -0.36 instead of -0.73 (see Figure 1 and Table 2). It is then evident that the virial product is significantly better correlated with the AGN variability than the luminosity alone.

Slightly better results are obtained if the intrinsic 2-10 keV luminosity, L_X, instead of the optical luminosity, L_{5100}, is used to compute the virial product. In this case the total and intrinsic spreads are 1.06 dex and 0.93 dex, respectively (see Figure 1 and Table 2). Also in this case the virial product is better correlated with $\sigma^2_{\rm rms}$ (r=-0.81 and probability 5×10^{-10}) than L_X alone is (r=-0.57 and spread 1.36 dex).

Finally, if the virial product is computed using L_X and Paβ, the spreads considerably decrease down to 0.71 dex (total) and 0.56 dex (intrinsic), while the correlation coefficient results to be r= -0.82 with a probability of 3×10^{-5} (see Table 2 and Figure 1). The correlation between L_X only and $\sigma^2_{\rm rms}$ has instead a less significant coefficient r= -0.63 (probability 4×10^{-3}) and a larger spread of 1.33 dex.

5. DISCUSSION AND CONCLUSIONS

The above described fits show that, as expected, highly significant relationships exist between the virial products and the AGN X-ray flux variability. These relationships allow us to predict the AGN 2-10 keV luminosities. The less scattered relation has a spread of 0.6-0.7 dex and is

[1] We preferred to look for the dependence of the square of the virial product from $\sigma^2_{\rm rms}$, instead of using eq. 6, in order to have comparable uncertainties on both axes (see Fig. 1).

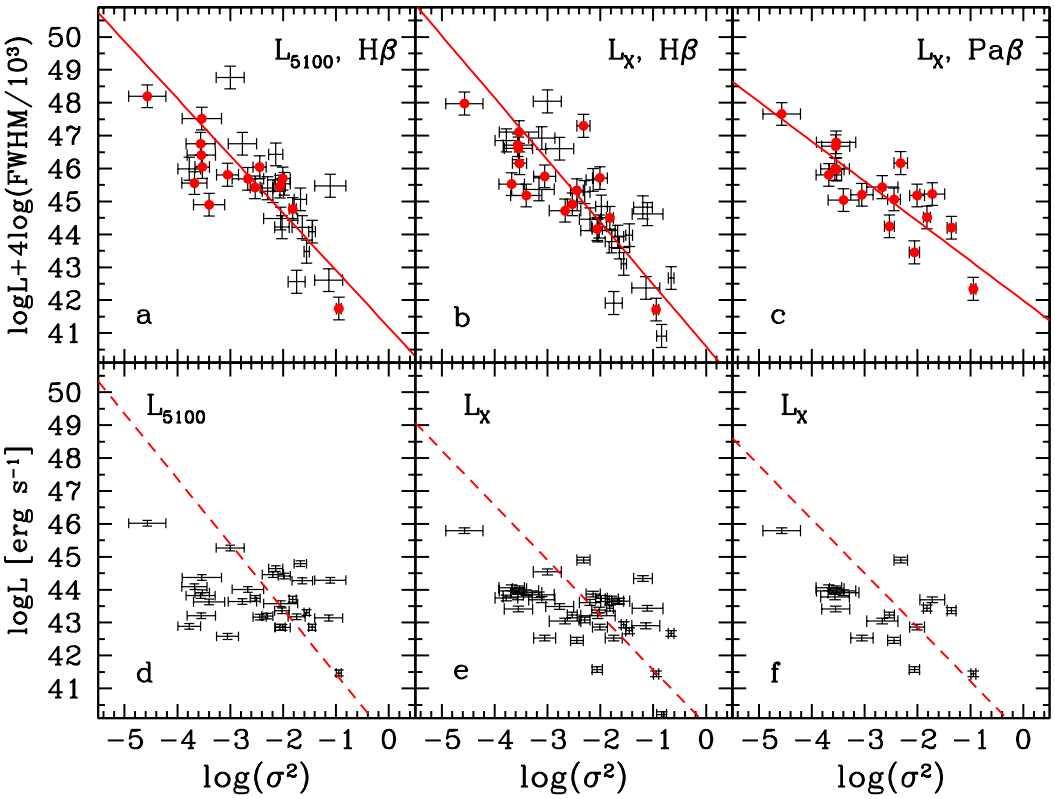

FIG. 1.— (a) Square of the virial product (computed using L_{5100} and $FWHM_{H\beta}$) as a function of the excess variance, σ^2_{rms}, of the 2-10 keV flux measured into 20 ks long bins. The continuous lines show the fit to the data (see Table 2). The objects having the Paβ FWHM measures available are shown by red filled circles. (b) As in the previous panel using L_X and $FWHM_{H\beta}$. (c) As in the previous panel using L_X and $FWHM_{Pa\beta}$. (d) L_{5100} as a function of σ^2_{rms} of the same sample shown in the upper panel. (e) L_X as a function of σ^2_{rms} of the same sample shown in the upper panel. (f) L_X as a function of σ^2_{rms} of the same sample shown in the upper panel. The dashed lines show the best fits to the data (see Table 2).

TABLE 2
PARAMETERS OF THE FITS

Variables	α	β	N. Obj	r	Prob(r)	Spread dex	Intrinsic Spread dex
(1)	(2)	(3)	(4)	(5)	(6)	(7)	(8)
L_{5100}, H_β	-1.74±0.13	41.17±0.29	31	-0.734	3×10^{-6}	1.12	1.00
L_{5100}	-1.98±0.11	39.45±0.20	31	-0.363	5×10^{-2}	1.78	1.72
L_X, H_β	-1.89±0.10	40.59±0.23	38	-0.813	5×10^{-10}	1.06	0.93
L_X	-1.67±0.07	39.90±0.12	38	-0.570	2×10^{-4}	1.36	1.32
L_X, Pa_β	-1.21±0.12	41.99±0.31	18	-0.822	3×10^{-5}	0.71	0.56
L_X	-1.64±0.09	39.58±0.18	18	-0.634	5×10^{-3}	1.33	1.28

NOTE. — Column 1: variables used to compute either the virial product or the luminosity. Columns 2 and 3: best fit parameters of eq. 7. Column 4: number of objects used. Column 5: correlation coefficient. Column 6: probability of the correlation coefficient. Column 7: logarithmic spread of the data on the y axis. Column 8: intrinsic logarithmic spread of the data on the y axis.

obtained when the Paβ line width is used. This could be due either because the Paβ broad emission line, contrary to Hβ, is observed to be practically unblended with other chemical species, or because, as our analysis is based on a collection of data from public archives, the Paβ line widths, which comes from the same project (Landt et al. 2008, 2013), could have therefore been measured in a more homogeneous way. In this case, it is then probable that new dedicated homogeneous observing programs could obtain even less scattered calibrations; at least for the Hβ-based relationships discussed in this work.

In order to use this method to measure the cosmological distances and then the curvature of the Universe, it is necessary to obtain reliable variability measures, corrected for the cosmological time-dilation, at relevant redshifts. In this respect, the relations based on the Hβ line width measurement are the most promising as can be used even up to redshift $\sim$3 via near infra-red spectro-

scopic observations (e.g. in the 1-5 μm wavelength range with NIRSpec[2] on the *James Webb Space Telescope*). Moreover, recent studies by Lanzuisi et al. (2014) suggest that previous claims of a dependence on redshift of the AGN X-ray variability should be attributed to selection effects.

Our AGN-based relations constitute a distance indicator alternative to SNeIa and GRB, that can be used to cross-check their distance estimates, revealing potential unknown sources of systematic errors in their calibration and improve the constraints on fundamental cosmological parameters including dark energy properties. To assess cosmological relevance of our distance estimate we compare, in Figure 2, the luminosity distance, D_L, of our estimator (blue dots) with two different sets of cosmological models. The first one refers to flat ΛCDM models allowed by the Union2.1 compilation of SNeIa (Suzuki et al. 2012). The black curve represents the best fit, while the red dashed and dotted curves are the $\pm1\sigma$ bounds. The corresponding values for $\Omega_{\rm M}$ are indicated in the plot. The second sets of curves represent a flat Dark Energy models with a non-evolving equation of state (wCDM), i.e. with constant w-parameter ($w \equiv p/\rho$), consistent with both the Planck maps and galaxy clustering in the BOSS survey (Sánchez et al. 2013), but with no reference to SNeIa data. The two blue dot-dashed and dashed curves represent $\pm1\sigma$ bounds with cosmological parameters indicated in the plot.

From a cosmological viewpoint our present application should be considered as a proof of concept that, however, can be developed by future missions such as the new mission concept *Athena* (recently proposed to the European Space Agency; Nandra et al. 2013). As $D_{\rm L}$ is proportional to the square root of the luminosity, the 0.7 dex uncertainty on the prediction of the AGN X-ray luminosity corresponds to a 0.35 dex uncertainty on the $D_{\rm L}$ measurement (see lower right corner in the upper panel of Figure 2)[3]. This implies that, if log-normal errors are assumed, variability measures of samples containing a number of AGN, $N_{\rm AGN}$, all having similar redshifts, will provide measures of the distance (at that average redshift) with uncertainties of $\sim 0.35/\sqrt{N_{\rm AGN}}$ dex. From Vaughan et al. (2003), in low signal-to-noise measurement conditions (when the Poissonian noise dominates), the excess variance measurement is larger than the noise when

$$\sigma^2_{\rm rms} > \sqrt{\frac{2}{\rm N}}\frac{1}{\mu t_o}, \qquad (9)$$

where N is the number of t_o long time intervals, and μ is the average count rate in ph/s units. As also confirmed by our data, the above formula requires a count rate $\mu \sim 1$ ph/s and 80 bins, $t_o = 250$ s long, in order to measure $\sigma^2_{\rm rms}$ larger than $\sim 5 \times 10^{-4}$ (as mainly observed in this work). If *Athena* will be used, $\mu \sim 1$ ph/s corresponds to a 2-10 keV flux of 10^{-13} erg s^{-1} cm^{-2}. According to the AGN X-ray luminosity function (La Franca et al. 2005; Gilli et al. 2007), at these fluxes, with a 10 Ms survey covering 250 deg^2 with 500 pointings of the Wide Field Instrument ($\sim$0.5 deg^2 large field of view), it will be possible to measure $\sigma^2_{\rm rms}$ in a sample of $\sim$250 unabsorbed ($N_{\rm H} < 10^{21}$ cm^{-2}) AGN contained in each of the redshifts bins $0< z <0.3$ and $0.3< z <0.6$, and a sample of $\sim$35 AGN in the redshift bin $0.6< z <0.9$. In this case $D_{\rm L}$ could be measured with a 0.02 dex uncertainty (0.1 mag) at redshifts less than 0.6, and with a 0.06 dex (0.3 mag) uncertainty in the $0.6< z <0.9$ bin (red error-bars in Figure 2). With the proposed *Athena* survey our estimator will not be competitive with SNeIa. It will, however, provide a cosmological test independent from SNeIa able to detect possible systematic errors if larger than 0.1 mag in the redshift range $z < 0.6$. A value a factor of ~ 4 more precise than the other alternative estimator based on the GRBs (Schaefer 2007).

In order to significantly exploit at higher redshifts our proposed $\sigma^2_{\rm rms}$-based AGN luminosity indicator to constraint the Universe geometry a further step is necessary, such as a dedicated Wide Field X-ray Telescope

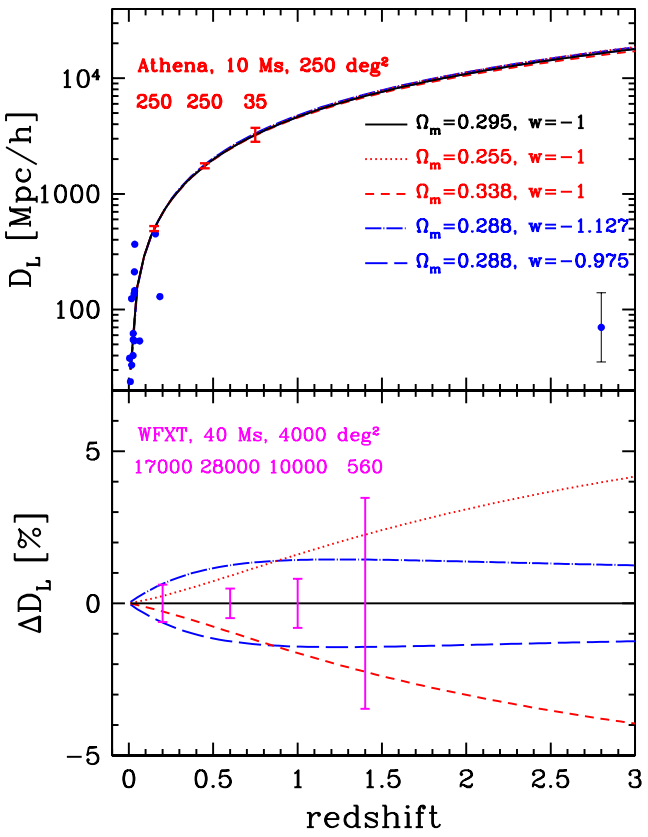

FIG. 2.— *Top.* Luminosity distance as a function of redshift. The curves represent cosmological models allowed by different datasets described in the text. Our measures, using L_X and Paβ, are shown by blue dots. On the lower right corner the typical uncertainty on a single measurement is shown. Red error bars show the expected uncertainties from a survey carried out with *Athena*. The expected number of AGNs in each of the 0.4-wide redshift bins is also shown. *Bottom.* Percent differences of the various cosmological models compared to their respective best fit. Magenta error bars show the expected uncertainties from a survey carried out with a future WFXT as described in the text. The expected number of AGNs in each of the 0.3-wide redshift bins is also shown.

[2] See `http://www.stsci.edu/jwst/instruments/nirspec`

[3] The logarithmic uncertainties on $D_{\rm L}$ should be multiplied by a factor 5 to convert them into distance modulus, ΔM, units.

(WFXT) with an effective collecting area at least three times larger than *Athena* and $\sim$2 deg^2 large field of view[4]. In this case, as an example, with a 40 Ms long program it would be possible to measure D_L with less than 0.003 dex (0.015 mag) uncertainties at redshift below 1.2 and an uncertainty of less than 0.02 dex (0.1 mag) in the redshift range $1.2 < z < 1.6$. The bottom panel of Figure 2 illustrates more clearly the potential of our new estimator. The curves represent the per cent difference of the luminosity distance models shown in the upper panel with respect to its reference best fit scenario. From the comparison between the magenta error-bars with the model scatter, we conclude that our estimator has the prospect to become a cosmological probe even more sensitive than current SNeIa if applied to AGN samples as large as that of an hypothetical future survey carried out with a dedicated WFXT as described above.

We thanks Federico Marulli for having helped us in the production of the luminosity distance dependences on redshift as a function of the cosmological models shown in this work. Paola Marziani, Dario Trevese and Fausto Vagnetti are acknowledged for useful discussions. Francesca Onori and Federica Ricci are acknowledged for having contributed in the archival data research, suggestions and carefully reading the manuscript. GP acknowledges support via an EU Marie Curie Intra-European fellowship under contract FP-PEOPLE-2012-IEF-331095. This project was supported by the international mobility program of University Roma Tre. We acknowledge funding from PRIN/MIUR-2010 award 2010NHBSBE. We would like to thank the referee for helpful comments.

REFERENCES

Assef, R. J., Frank, S., Grier, C. J., et al. 2012, ApJ, 753, L2
Baldwin, J. A. 1977, ApJ, 214, 679
Bentz, M. C., Denney, K. D., Grier, C. J., et al. 2013, ApJ, 767, 149
Boller, T., Brandt, W. N., & Fink, H. 1996, A&A, 305, 53
Collier, S., Horne, K., Wanders, I., & Peterson, B. M. 1999, MNRAS, 302, L24
Conconi, P., Campana, S., Tagliaferri, G., et al. 2010, MNRAS, 405, 877
Denney, K. D., Peterson, B. M., Dietrich, M., Vestergaard, M., & Bentz, M. C. 2009, ApJ, 692, 246
Elvis, M., & Karovska, M. 2002, ApJ, 581, L67
Gierliński, M., Nikołajuk, M., & Czerny, B. 2008, MNRAS, 383, 741
Gilli, R., Comastri, A., & Hasinger, G. 2007, A&A, 463, 79
Grupe, D., Beuermann, K., Mannheim, K., & Thomas, H.-C. 1999, A&A, 350, 805
Grupe, D., Wills, B. J., Leighly, K. M., & Meusinger, H. 2004, AJ, 127, 156
Jin, C., Ward, M., Done, C., & Gelbord, J. 2012, MNRAS, 420, 1825
Kelly, B. C., Treu, T., Malkan, M., Pancoast, A., & Woo, J.-H. 2013, ApJ, 779, 187
Kraemer, S. B., Turner, T. J., Crenshaw, D. M., & George, I. M. 1999, ApJ, 519, 69
La Franca, F., Fiore, F., Comastri, A., et al. 2005, ApJ, 635, 864
Landt, H., Bentz, M. C., Ward, M. J., et al. 2008, ApJS, 174, 282
Landt, H., Ward, M. J., Peterson, B. M., et al. 2013, MNRAS, 432, 113
Lanzuisi, G., Ponti, G., Salvato, M., et al. 2014, ApJ, 781, 105
Leighly, K. M. 1999, ApJS, 125, 317
Marziani, P., & Sulentic, J. W. 2013, arXiv:1310.3143
McHardy, I. M., Gunn, K. F., Uttley, P., & Goad, M. R. 2005, MNRAS, 359, 1469
McHardy, I. M., Koerding, E., Knigge, C., Uttley, P., & Fender, R. P. 2006, Nature, 444, 730
McLure, R. J., & Dunlop, J. S. 2001, MNRAS, 327, 199
McLure, R. J., & Jarvis, M. J. 2002, MNRAS, 337, 109
Nandra, K., Mushotzky, R. F., Yaqoob, T., George, I. M., & Turner, T. J. 1997, MNRAS, 284, L7
Nandra, K., Barret, D., Barcons, X., et al. 2013, ArXiv e-prints, arXiv:1306.2307
O'Neill, P. M., Nandra, K., Papadakis, I. E., & Turner, T. J. 2005, MNRAS, 358, 1405
Perlmutter, S., Aldering, G., Goldhaber, G., et al. 1999, ApJ, 517, 565
Ponti, G., Papadakis, I., Bianchi, S., et al. 2012, A&A, 542, A83
Press, W. H., Teukolsky, S. A., Vetterling, W. T., & Flannery, B. P. 2007, Numerical recipes: the art of scientific computing, 3rd edn. (Cambridge Univ. Press, Cambridge)
Riess, A. G., Filippenko, A. V., Challis, P., et al. 1998, AJ, 116, 1009
Rubin, D., Knop, R. A., Rykoff, E., et al. 2013, ApJ, 763, 35
Rudge, C. M., & Raine, D. J. 1999, MNRAS, 308, 1150
Sánchez, A. G., Kazin, E. A., Beutler, F., et al. 2013, MNRAS, 433, 1202
Schaefer, B. E. 2007, ApJ, 660, 16
Shemmer, O., Brandt, W. N., Paolillo, M., et al. 2014, ArXiv e-prints, arXiv:1401.5496
Suzuki, N., Rubin, D., Lidman, C., et al. 2012, ApJ, 746, 85
Torres, C. A. O., Quast, G. R., Coziol, R., et al. 1997, ApJ, 488, L19
Turner, T. J., George, I. M., Nandra, K., & Turcan, D. 1999, ApJ, 524, 667
Vaughan, S., Edelson, R., Warwick, R. S., & Uttley, P. 2003, MNRAS, 345, 1271
Vestergaard, M., & Osmer, P. S. 2009, ApJ, 699, 800
Vestergaard, M., & Peterson, B. M. 2006, ApJ, 641, 689
Wandel, A., Peterson, B. M., & Malkan, M. A. 1999, ApJ, 526, 579
Wang, J.-M., Du, P., Valls-Gabaud, D., Hu, C., & Netzer, H. 2013, Physical Review Letters, 110, 081301
Watson, D., Denney, K. D., Vestergaard, M., & Davis, T. M. 2011, ApJ, 740, L49
Winkler, H. 1992, MNRAS, 257, 677
Zhou, H., Wang, T., Yuan, W., et al. 2006, ApJS, 166, 128
Zhou, X.-L., Zhang, S.-N., Wang, D.-X., & Zhu, L. 2010, ApJ, 710, 16

[4] A similar kind of mission has already been proposed (Conconi et al. 2010, see also: `http://wfxt.pha.jhu.edu/index.html`).